RSC Advances

PAPER

View Article Online
View Journal | View Issue

Cite this: *RSC Adv.*, 2018, **8**, 31081

A relationship between the V^{4+}/V^{5+} ratio and the surface dispersion, surface acidity, and redox performance of V_2O_5–WO_3/TiO_2 SCR catalysts

Xuteng Zhao, [a] Yongyi Yan,[a] Lei Mao, [a] Maochen Fu,[a] Hairui Zhao,[a] Lvsheng Sun,[a] Youhong Xiao[b] and Guojun Dong *[a]

Received 3rd April 2018
Accepted 10th August 2018

DOI: 10.1039/c8ra02857e

rsc.li/rsc-advances

A series of V_2O_5–WO_3/TiO_2 catalysts with different vanadium loading amounts were prepared by an impregnation method and were characterized by XRD, Raman spectroscopy, XPS, DRIFTS, Py-DRIFTS, NH_3-TPD, H_2-TPR, *etc.* The results show that the catalytic activity is related to the ratio of V^{4+}/V^{5+}. The variation of the V^{4+}/V^{5+} ratio caused by the different dispersion states of vanadia oxide leads to changes in the surface acidity and redox properties of the catalysts. As the V^{4+}/V^{5+} ratio reaches the maximum value, the apparent activation energy (E_a) required to form the transition state on the Brønsted acid sites is the lowest. Artificial regulation of vanadium loading to properly increase V^{4+}/V^{5+} content may affect the interactions between V, W, O and Ti atoms, which enhances NH_3-SCR reaction performance.

1 Introduction

Nitrogen oxides (NO_x) cause many environmental issues, such as photochemical smog, acid rain, ozone depletion and the greenhouse effect. NH_3 selective catalytic reduction (SCR) has attracted numerous researchers, who are showing interest in effective and fundamental technological applications of this reaction in environmental purification.[1–3] It is necessary to pursue higher deNO_x activity for the SCR catalysts used for mobile sources at low temperature on account of the relatively low temperature of exhaust gas. Thus, low-temperature SCR catalysts should be researched further. The V_2O_5–WO_3/TiO_2 catalyst system has been the most widely used catalyst in industrial applications for decades. Although this catalyst system is very old, it is still widely applied.[4,5] It is known that V_2O_5–WO_3/TiO_2 catalysts exhibit high efficiency at 300 °C to 450 °C[6] and V_2O_5–WO_3/TiO_2 catalysts with higher vanadium contents show much better catalytic performance at low temperature.[2,7] However, excessive vanadium species not only generate large amounts of N_2O by-products but are also volatilized during the catalyst operation, which is very hazardous to the environment and human health.[6] Hence, it is necessary to clarify the operation mode of vanadium species on the catalyst surface.

V_2O_5 is the active component and WO_3 is the accelerator and stabilizer on a V_2O_5–WO_3/TiO_2 catalyst.[8] Vanadium oxide surface sites are very active in the adsorption of organic molecules. This process follows a Mars-van Krevelen mechanism, where the adsorbed organic molecule is oxidized *via* reduction of the superficial metal cation.[9–11,13] Ammonia is also readily and strongly adsorbed on the vanadium active sites.[13] Many reports show that a variety of oxidation states of vanadium oxide can improve the catalytic activity; this is attributed to the rapid redox cycle of vanadium oxide.

The denitration activity of a VO_x species has a relationship with its structure. Cai *et al.*[12] found that the optimum vanadia loading appeared to fall between monolayer coverage and crystalline V_2O_5. By using structural calculations,[14] with the condition that the surface monolayer vanadia has a similar molecular structure to crystalline V_2O_5, the monolayer surface coverage of V_2O_5 was estimated to be about 10 VOx per nm^2. Furthermore, Deo *et al.*[15] found that the monolayer surface coverage of vanadia is approximately 7 to 8 VO_x per nm^2 when the vanadia species is isolated on different carriers. However, Raman spectroscopy is sensitive to crystalline V_2O_5 and amorphous vanadia. By combining Raman spectroscopy with oxygen-18 isotopic labeling experiments, it can be illustrated that isolated vanadia species possess a terminal V=O bond and three bridging V–O–Ti bonds; also, the polymerized species possesses a terminal V=O bond, a bridging V–O–Ti bond and two bridging V–O–V bonds.[16] Researchers have suggested that V_2O_5 has three states on the catalyst surface: monomeric vanadium species, polymeric vanadium species and crystalline vanadium species. Increasing the vanadia oxide loading amount can promote the transfer of monomeric vanadium species to polymeric and crystalline vanadium species.[17,18] G. T. Went *et al.*[19] suggested that polymeric vanadium species possess the highest catalytic activity based on *in situ* Raman studies; this activity is more than 10 times greater than that of the monomeric vanadium species in the NH_3-SCR reaction.

[a]*College of Materials Science and Chemical Engineering, Key Laboratory of Superlight Materials and Surface Technology of Education Ministry, Harbin Engineering University, Harbin, 150001, China. E-mail: dgj1129@163.com*

[b]*College of Power and Energy Engineering of Harbin Engineering University, Harbin, 150001, China*

In our previous work, we adjusted the $(V^{4+} + V^{3+})/V^{5+}$ or V^{4+}/V^{5+} ratio by changing the pH value; the results demonstrated that the catalyst with the optimal performance of the best NO_x conversion and N_2 selectivity contained highly coordinated polymeric vanadia species when the amount of low valence state V was increased.[20] Furthermore, according to our research on adjusting the $(V^{4+} + V^{3+})/V^{5+}$ or V^{4+}/V^{5+} ratio *via* changing the oxygen flux in the calcining process, we found that the V^{4+}/V^{5+} ratio increased in an appropriate range; the amount of polymeric vanadia species also increased and E_a decreased.[21] A report by M. J. Lázaro *et al.*[22] showed that NO conversion reached a maximum because the vanadia-based catalyst has a higher Brønsted proton acid (V^{4+}) concentration. The surface coverage of a sample doped with tungsten and vanadia reached approximately half a monolayer, and the higher NO conversion had a close relationship with the well-dispersed and dissociated vanadia species. It can be inferred that the Brønsted proton acid (V^{4+}) variation is related to the structure variation of the vanadia species.

In the above reports, we can infer that relative content of active components in different valence states has a significant effect on the NO conversion. However, although the VWTi catalytic system has been studied for many years, there are few reports about the detailed relationship between the V^{4+}/V^{5+} ratio and the dispersion state, surface acidity, adsorbed oxygen concentration and redox properties of this system. In this study, the vanadium content with different valencies on the support surface was controlled by adjusting the vanadium loading, and the relationship between the V^{4+}/V^{5+} ratio and the influence of the relative content of vanadium species with different valence states on NO conversion was researched by XRD, Raman spectroscopy, XPS, *in situ* infrared spectroscopy, DRIFTS, *etc.*

2 Experimental

2.1 Catalyst preparation

A series of catalyst samples were prepared by the substep-wet impregnation method. All chemicals were analytical reagent grate. Commercial anatase TiO_2 ($S_{BET} = 120\ m^2\ g^{-1}$, Tianjing Guangfu Material Company) was added to a solution containing an appropriate amount of ammonium paratungstate dissolved in oxalic acid solution. After the solution was stirred for 24 h, the mixed solution was then heated at 100 °C for 2 h to remove water to obtain the dry solid product, which was then dried at 120 °C overnight and finally calcined in air at 500 °C for 3 h to obtain 8 wt% WO_3/TiO_2 support. After that, using oxalic acid as solvent, an appropriate amount of ammonium metavanadate was dissolved in solution; then, WO_3–TiO_2 carrier was added to this solution and the previous drying and calcining steps were repeated. Using the above method, a series of $V_2O_5(n)WO_3/TiO_2$ catalysts were successfully prepared, where n indicates the V_2O_5 content expressed in wt%. All the samples are abbreviated to V*n*W/Ti ($n = 1$, 3, 5, 7, 9, 11 and 13).

2.2 Catalyst characterization

The XRD patterns were recorded on an X-ray diffractometer (Rigaku D/max-TTR-III) with Cu Kα radiation ($\lambda = 0.15405$ nm) operating at a scan rate of 10° min^{-1} with a 2θ angle range from 10° to 80°. The N_2 adsorption–desorption isotherms were acquired at −196 °C using a Builder SSA-4300 instrument (China, Builder Company). Raman spectra were recorded under dehydrated conditions with a resolution of 1 cm^{-1} and a 785 nm laser using a Microscopic Confocal Raman Spectrometer (Perkin Elmer, station 400F). The X-ray photoelectron spectra (XPS) were recorded on a K-Alpha spectrometer (Thermo Fisher SCIENTIFIC, America) equipped with an Al Kα radiation (1486.6 eV) X-ray source.

The temperature programmed reduction (TPR) was measured on a PCA 1000 automatic chemical adsorption instrument with a thermal conductivity detector (TCD). Firstly, 0.1 g catalyst was treated with an ultra-high-purity argon (30 mL min^{-1}) flow at 50 °C for 30 min. Then, the reactor was heated from 50 °C to 800 °C at a rate of 10 °C min^{-1} under 5 vol% H_2/Ar (30 mL min^{-1}). The TPO test was performed after reduction of the sample with 5 vol% H_2/Ar from 50 °C to 600 °C. After that, all samples were retreated under pure Ar (30 mL min^{-1}) at 50 °C for 30 min; then, the TPO run was carried out in 5 vol% O_2/Ar with 30 mL min^{-1} flow by increasing the temperature from 50 °C to 800 °C at a rate of 10 °C min^{-1}.

The redox rate (in mol m^{-2} s^{-1}) mentioned here refers to the average reduction rate and the average oxidation rate in the reduction or oxidation process, described as the hydrogen consumption or the oxygen consumption for a unit area of the catalyst in a unit of time, respectively. The hydrogen consumption and the oxygen consumption were obtained by calculating the peak area based on the TPR of standard CuO and the TPO of standard Cu. The slope of the TPO or TPR curve was described as the momentary rate of the oxidation or reduction process, respectively.

The NH_3 adsorption FTIR spectra were recorded in the range of 1000 to 4000 cm^{-1} using an FTIR spectrometer (Nicolet 6700) equipped with an MCT detector (100 scans, 4 cm^{-1} resolution). Prior to the measurement, all calcined catalyst samples were placed in a Harrick DRIFTS cell and purged with Ar at 300 °C for 1 h to remove surface organic residues. After the sample was cooled to room temperature, the background spectrum was collected under flowing argon. Then, the sample was exposed to 0.1% (v/v) NH_3/Ar (120 mL min^{-1}) for half an hour and subsequently flushed with Ar. Finally, the NH_3 adsorption FTIR spectra were collected. This device was also used for the *in situ* pyridine adsorption infrared test.

In order to further investigate the reactivity of adsorbed NH_3 on the catalyst, NH_3 *in situ* FTIR experiments were carried out using an FTIR spectrometer. The catalyst was purged in Ar (50 mL min^{-1}) at 400 °C for 1 h, then cooled to 200 °C. The NH_3 adsorption was carried out in 1000 ppm NH_3/Ar (50 mL min^{-1}) for 30 min; then, mixed gas of 1000 ppm NO/Ar and 5% O_2 was used to react with the adsorbed ammonia on the catalyst surface. *In situ* FTIR spectra of the catalysts were collected at various times.

NH_3-TPD measurements were carried out using a PCA 1000 automatic chemical adsorption instrument with a thermal conductivity detector (TCD). 0.1 g sample was packed in a quartz tube, treated at 400 °C for 30 min with Ar, and cooled to

50 °C; then, pure NH_3 was adsorbed on the catalyst surface for 10 minutes. Then, the samples were ramped to 600 °C at a rate of 10 °C min^{-1} to desorb NH_3.

2.3 Catalytic activity

The NH_3-SCR activities of the catalysts were determined in a fixed-bed quartz tubular microreactor with the inlet and outlet gases monitored by a PFEIFFER GSD320 gas analysis system (ThermoStarTM, Germany). The 0.6 g catalyst sample was evaluated under simulated exhaust gas: 1000 ppm NO, 1000 ppm NH_3, 5% O_2/Ar and balance Ar. The total gas flow rate was 200 mL min^{-1}, corresponding to a gas hourly space velocity (GHSV) of 20 000 h^{-1}. Prior to each experiment, the catalyst was purged with an Ar flow at 250 °C for 1 h, and the activity test was performed at atmospheric pressure from 150 °C to 410 °C at a heating rate of 10 °C min^{-1}. The NO_x conversion (%) was obtained using the following eqn (1):

$$NO_x \text{ conversion } (\%) = \frac{[NO]_{in} - [NO]_{out} - [NO_2]_{out} - 2[N_2O]_{out}}{[NO]_{in}} \times 100\% \quad (1)$$

3 Results and discussion

3.1 Surface structure analysis

Fig. 1 shows the XRD patterns of the V*n*W/Ti catalysts with different vanadia loading amounts. The XRD patterns of the samples are mainly attributed to anatase phase TiO_2 (JCPDS, PDF 21-1272). No obvious V_2O_5 crystal diffraction peak appears when the vanadium content is less than 9%, which shows that no crystalline vanadium oxide is generated under this condition. However, two weak diffraction peaks attributed to crystalline V_2O_5 appear at 26.1° and 20.3° in the spectra of V11W/Ti and V13W/Ti. The formation of crystalline vanadium oxides is a process of aggregation state transition. It has been reported that vanadia species transform from tetrahedral VO_4 (ref. 23 and 24) to moderately distorted dimeric or oligomeric species,[25,26] then to isolated polymers[27] and finally to crystalline V_2O_5.[28] In this work, with increasing vanadium content, the vanadium oxide gradually changes from a dispersed state to an aggregated state and finally forms crystals. It can be inferred that vanadium oxide in V9W/Ti may exist in the form of an intermediate state of aggregation; in addition, according to the catalytic activity tests, V9W/Ti has the best catalytic activity. Therefore, the presence of transitional state oxides may improve the catalytic activity. To further verify the existence of this transitional state, the number of atoms per unit area have been calculated as follows (2).[30]

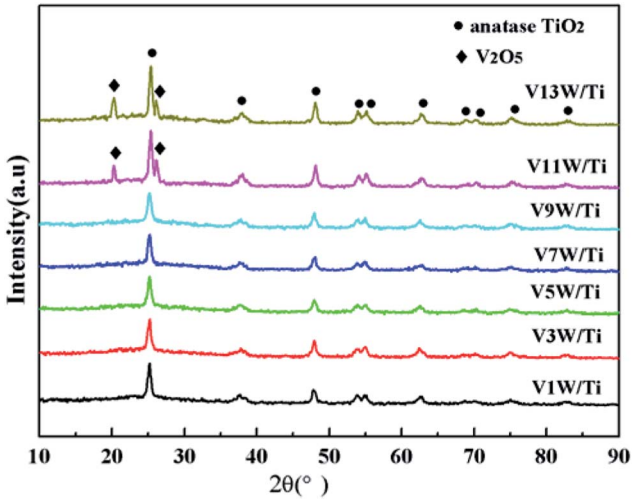

Fig. 1 XRD patterns of the V*n*W/Ti catalysts.

$$N_{number} = \frac{WN_A}{MA_{BET}} \quad (2)$$

Here, N_{number} denotes the atomic number of the element per unit area, W represents the percentage composition of elements, N_A is Avogadro's constant, M is the relative atomic mass of the element, and A_{BET} is the BET specific surface area.

The BET results, crystallite sizes of V_2O_5, percentages of vanadium atom and V atomic numbers per unit area of the V*n*W/Ti catalysts have been summarized in Table 1. The monolayer surface coverage of the vanadia oxide overlayer on different oxide supports has been found to be approximately 7 to 8 atoms per nm^2; this monolayer coverage corresponds to 6 wt% V_2O_5 on the TiO_2 support.[31] The number of vanadium atoms in the V9W/Ti catalyst is approximately 8.4/nm^2. Obviously, increasing the vanadium content and the addition of tungsten slightly increase the content of V dispersed on the support surface. Additionally, the large increase of N_{number} and the sum of the V atoms in V11W/Ti and V13W/Ti proves the formation of crystalline vanadium. These results indicate that vanadium oxide may be in a transitional state from the dispersed state to the crystalline state in the V9W/Ti catalyst. Interestingly, although the amount of tungsten was not changed, the number of tungsten atoms increased sharply when the crystalline vanadium oxide was formed; this indicates that the dispersion of tungsten oxide on the support surface was also changed by the formation of crystalline vanadium oxide.

The specific surface area of V1W/Ti–V9W/Ti decreases slightly with increasing vanadium loading amount. However, V9W/Ti exhibits the best catalytic performance. It should be noted that the specific surface area decreases significantly in V11W/Ti and V13W/Ti, which can be attributed to the formation of crystalline V_2O_5. It can be inferred that the catalytic activity is not affected by a decrease in specific surface area in this catalytic system.

Although the formation of crystalline V_2O_5 was detected in the XRD patterns, the detailed structural characteristics of the vanadate species could not be determined from the XRD results. Therefore, Raman spectra were used to study the structural characteristics of the vanadium species in the V*n*W/Ti samples (Fig. 2).

V–O, W–O, V=O and W=O on the catalyst surface changed with increasing loading amount of vanadium. The peaks at 396,

Table 1 Specific surface areas, surface atoms and valence states of elements and ratios of the V*n*W/Ti catalysts

Sample	Specific surface area ($m^2\ g^{-1}$)	Percentage of V atom (at% by XPS)	Atomic number (nm^{-2})		V2p		W4f	O1s	Crystallite size of V_2O_5 (nm)
			V	W	V^{4+}/V^{5+}	$(V^{4+} + V^{3+})/V$	W^{6+}/W	$O_\alpha/(O_\alpha + O_\beta)$	
TiO_2	120	—	—						
W/Ti	77.45	—	—	2.5					
V1W/Ti	73.50	0.62	0.8	2.6	0.49	0.41	0.55	0.23	—
V3W/Ti	68.39	0.80	2.6	2.7	0.53	0.41	0.63	0.28	—
V5W/Ti	65.13	1.48	4.5	2.8	0.99	0.52	0.68	0.34	—
V7W/Ti	60.91	1.52	6.6	2.9	1.47	0.61	0.71	0.36	—
V9W/Ti	60.68	2.28	8.4	2.9	1.73	0.64	0.93	0.38	—
V11W/Ti	30.13	2.94	20.3	5.6	0.88	0.56	0.81	0.31	14.1
V13W/Ti	26.15	3.54	27.1	6.5	0.50	0.49	0.69	0.30	15.5

514 and 638 cm^{-1} shown in Fig. 2(a) are attributed to the symmetrical stretching vibration and the symmetrical and unsymmetrical bending vibrations of anatase TiO_2, respectively.[32] Also, the peaks at 1074 to 1112 cm^{-1} in Fig. 2(b) are attributed to the V=O stretching vibration.[27] The relative strengths of the interactions between V, W and O change, with slight shifts in the wavenumbers of the individual peak positions. No peaks of V=O and V–O appear in the spectrum of the W/Ti catalyst. When the vanadium content is low, the interaction between vanadium species and the catalyst support is mainly represented by O=V–O–Ti^{4+}. With increasing vanadium loading amount, the vanadium species transition from a dispersed state to a concentrated state; the wavenumbers of the V=O bond increase gradually from V1W/Ti to V11W/Ti and decrease sharply from V11W/Ti to V13W/Ti, corresponding to the same trend of interaction strength of the V=O bonds, and O=V–O–V^{4+}(V^{5+})–O–Ti^{4+} will also form. The radii of V^{4+} (53 pm) and V^{5+} (46 pm) are very close to the radius of Ti^{4+} (51 pm), and they exhibit a strong ability to attract electrons; thus, the attraction between V and O atoms in V=O is enhanced. When the vanadium loading reaches 9%, the support surface is occupied by a large number of aggregated vanadium species, resulting in a suppression effect of the V=O stretching vibration and an increase in the interaction strength of the V=O

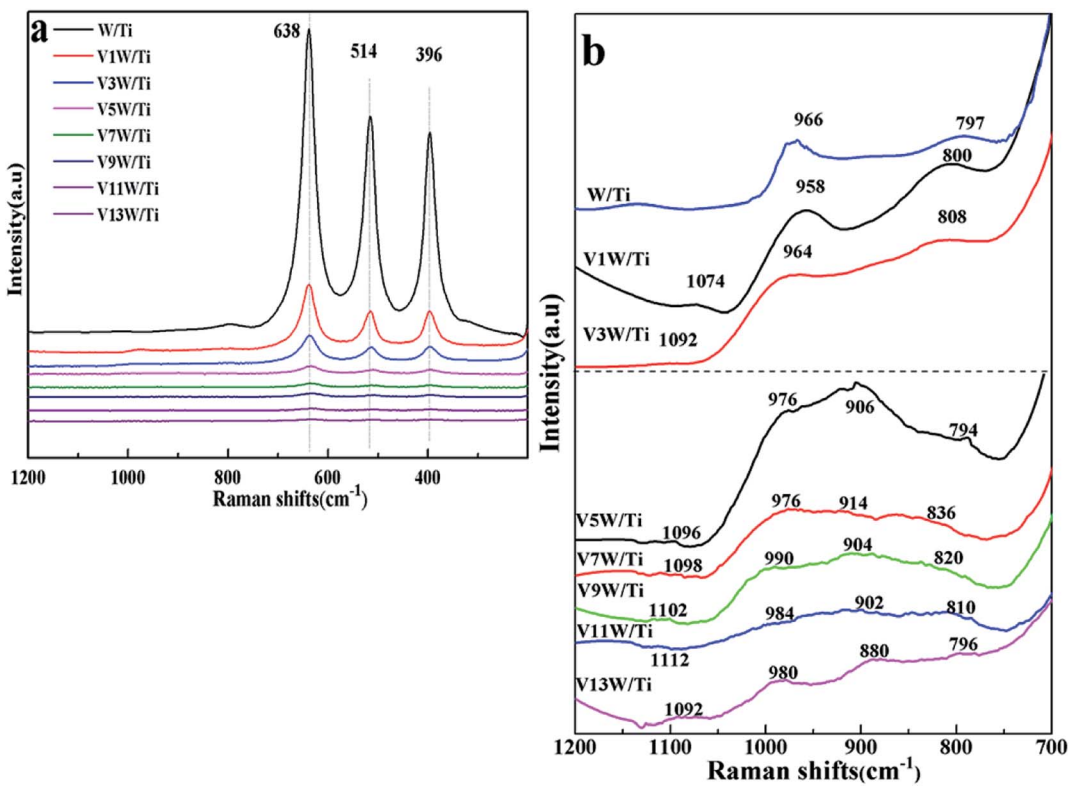

Fig. 2 Raman spectra of the V*n*W/Ti catalysts ((a) Raman bands in the 200 to 1200 cm^{-1} region; (b) Raman bands in the 700 to 1200 cm^{-1} region).

bond. Moreover, the sharp decreases of the wavenumbers in V11W/Ti and V13W/Ti are due to the formation of crystalline V_2O_5, which results in decreased V=O stretching vibrations and decreased interaction strength of the V=O bonds. Thus, it can be inferred that highly dispersed and crystalline vanadium species can promote V=O stretching vibrations and then decrease the energy required for the V=O stretching vibrations; however, aggregated and transition state vanadium species exhibit the opposite trend. The vanadium species may be in transition from the aggregation state to the crystalline state when the vanadium loading is between 5% and 9%. As the loading continues to increase, crystalline vanadium is generated on the surface. In addition, the peaks located at 958 to 990 cm^{-1} are attributed to the W=O bond.[33] Similarly, the frequencies of the W=O bond increase initially and then decrease. This indicates a changing trend of the interaction strength of the W=O bond. When the vanadium loading exceeds 5%, the W=O vibration is restrained and the interaction strength of the W=O bond increases. However, the formation of crystalline V_2O_5 in V11W/Ti to V13W/Ti inhibits the interactions between V and W atoms; thus, the W=O stretching vibration strengthens, resulting in a decrease of the interaction strength of the W=O bond.

The peaks located at 880 to 914 cm^{-1} and 794 to 836 cm^{-1} are attributed to the V–O bond[27] and W–O bond.[33] For V1W/Ti and V3W/Ti, no obvious V–O bonds are observed. However, V3W/Ti has an extremely weak peak at 900 cm^{-1} because of the formation of a small amount of the dimeric structural mode on the catalyst surface. In addition, due to the massive formation of V–O in V5W/Ti, the W–O frequencies decrease from 808 cm^{-1} to 794 cm^{-1}, which indicates that V–O has combined with W–O to form V–O–W.[34,35] This result causes enhancement of the W–O stretching vibration and a decrease of the interaction strength of the W–O bond. Moreover, the peaks of the V–O bond and W–O bond initially shift to higher Raman shifts in V5W/Ti to V7W/Ti and then to low frequencies in V9W/Ti to V13W/Ti. This indicates that V–O has combined with W–O to form V–O–W, resulting in red shifts of the V–O and W–O peaks in V9W/Ti to V13W/Ti; then, the formation of crystalline V_2O_5 enhances the trend of self-polymerization to form crystalline V_2O_5, and the V–O and W–O peaks thus shift to high frequencies. Based on the above results, it can be inferred that three valence states of vanadium lead to the formation of various VO_x species on the catalyst surface. When the vanadium content is less than 5%, the V species is mainly present as a single vanadium and is highly dispersed on the support surface; when the vanadium content is in the range of 5% to 9%, the V species begin to accumulate in large amounts and transition from the aggregation state to the crystalline state; when the vanadium content reaches 11%, a large number of crystalline vanadium species appear. More importantly, the difference caused by vanadium loading is reflected by the regular change of the V^{4+}/V^{5+} ratio, and the contents of V^{3+}, V^{4+} and V^{5+} change with variation of the vanadium dispersion state. Therefore, XPS tests were performed, and the results are as follows.

3.2 Valence states of vanadium and their ratios

The XPS results are summarized in Table 1 according to the peak-fit processing for the V2p spectra in Fig. 3(a). The vanadium species mainly exist on the catalyst surface as V^{5+}, V^{4+} and V^{3+}, with binding energies of 517.3 eV, 516.3 eV and 515.5 eV assigned to $V^{5+}2p_{3/2}$, $V^{4+}2p_{3/2}$ and $V^{3+}2p_{3/2}$, respectively.[36,37] With increasing vanadium loading, the contents of V^{4+} and V^{3+} also increase. When the vanadium loading reaches 9%, the amounts of V^{4+} and V^{3+} are the highest and the ratios of V^{4+}/V^{5+} and $(V^{4+}+V^{3+})/V^{5+}$ reach the maximum. The V^{4+}/V^{5+} ratio decreases in V11W/Ti and V13W/Ti because of the formation of the V^{5+}=O vanadium oxide species in the process of the formation of crystalline V_2O_5. Combined with the Raman test results, it can be inferred that the V species in the transition state between the aggregated and crystalline states will maintain a higher V^{4+}/V^{5+} ratio.

In Fig. 3(b), the tungsten species exist as W^{6+} ($W^{6+}4f_{7/2}$ = 35.75 eV, $W^{6+}4f_{5/2}$ = 37.7 eV) and W^{5+} ($W^{5+}4f_{7/2}$ = 34.9 eV, $W^{5+}4f_{5/2}$ = 36.7 eV) valence states, but are mainly in the form of

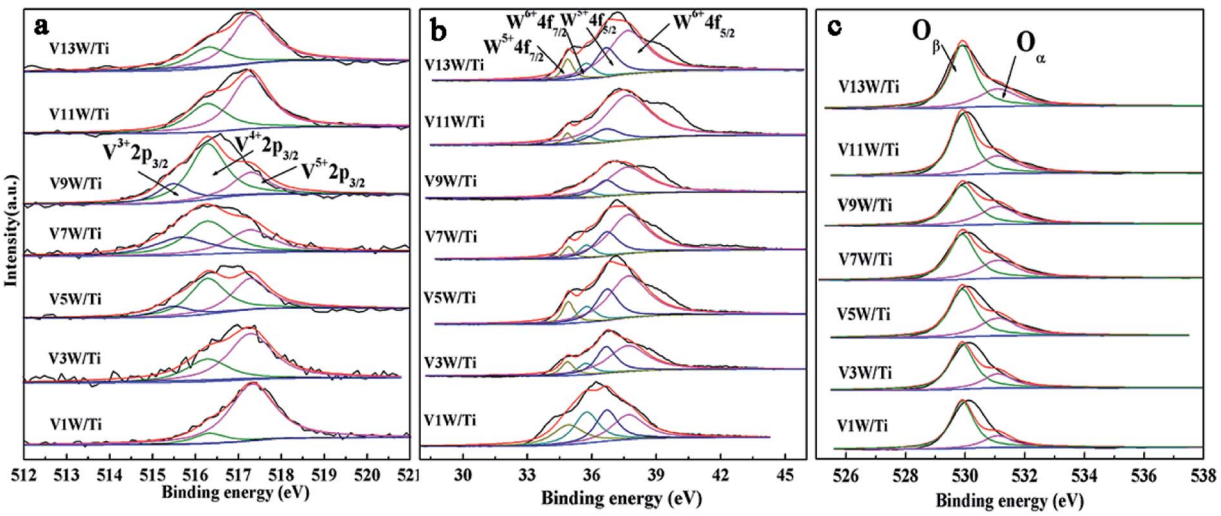

Fig. 3 V2p, W4f, and O1s XPS spectra of the V*n*W/Ti catalysts ((a) V2p; (b) W4f; (c) O1s).

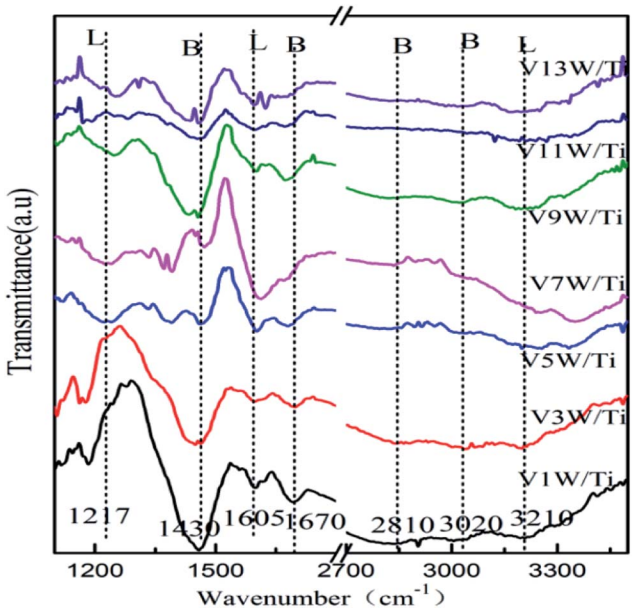

Fig. 4 IR spectra of the V*n*W/Ti catalysts with NH_3 adsorption at 50 °C.

W^{6+}. The addition of WO_3 is essential in this catalytic system. WO_3 has the effect of storing and transferring electrons to the vanadium oxide species, which can stabilize the valence states of V^{4+} and V^{3+}.[38,39] Thus, the V^{4+}/V^{5+} ratio also has a great relationship with the W^{6+}/W ratio. From Table 1, the valence states of W and V have the same trend. Interestingly, although the total amount of W has not changed, the content of W^{6+} changes with the vanadium loading. When the vanadium loading reaches 9%, the amounts of W^{6+} reach the maximum. It has been reported that an increase of V^{4+} is beneficial to the transition of tungsten to higher valence states to form V^{4+}–O–W^{6+}. Conversely, the increase of V^{5+} facilitates the transition of tungsten to low-valence states to form V^{5+}–O–W^{5+}.[34,35] Increasing the W^{6+} content is favorable for the SCR reaction,[40] and the V9W/Ti catalyst has the best catalytic activity according to the activity test results. It can be inferred that the changes in V^{4+}/V^{5+} caused by different loads will affect the content of W^{6+}.

The O1s peaks can be de-convoluted into two peaks: the lattice oxygen (O^{2-}) peak at 529.9 eV (denoted as O_β) and the chemisorbed oxygen (O_2^{2-}, O^-) peak at 531.1 eV (denoted as O_α), as shown in Fig. 3(c). Surface chemisorbed oxygen has been reported[41] to be the most active oxygen and plays an important role in oxidation reactions; also, a higher relative ratio of $O_\alpha/(O_\alpha + O_\beta)$ on the catalyst surface can be correlated with high SCR activity. From Table 1, the ratio of $O_\alpha/(O_\alpha + O_\beta)$ has the same trend as V^{4+}/V^{5+}. The highest ratio of $O_\alpha/(O_\alpha + O_\beta)$ is 0.38 in the V9W/Ti catalyst. This is consistent with the results of the activity tests. It can be inferred that there is a strong relationship between V^{4+}/V^{5+} and $O_\alpha/(O_\alpha + O_\beta)$. The same change trend of $O_\alpha/(O_\alpha + O_\beta)$ as V^{4+}/V^{5+} may be due to the increased oxygen defect concentration caused by the increase of V^{4+}/V^{5+}. Based on the above test results, although the contents of V^{4+} and V^{5+} gradually increase during the addition of vanadium, the difference in the ratio of V^{4+}/V^{5+} is a key factor in controlling the catalytic activity. The change trend of V^{4+}/V^{5+} is very close to the variation trend of the dispersion state of the vanadium species and the concentration of chemically adsorbed oxygen. The relationship between the V^{4+}/V^{5+} ratio and the changes in the surface acid sites will be further discussed below.

3.3 Surface acidity of catalysts

Surface acidity has a great influence on SCR reaction activity.[42] The changes in the V^{4+}/V^{5+} ratio caused by different loadings have great influence on the surface acidity in this catalytic system. The IR spectra of the V*n*W/Ti catalysts with NH_3 adsorption at 50 °C are shown in Fig. 4. The peaks at 3210, 1605 and 1217 cm^{-1} are attributed to ν_s(N–H), δ_{as}(H–N–H) and δ_{as}(H–N–H), corresponding to adsorption of NH_3 species on the Lewis acid sites of the catalyst surfaces, respectively. The peaks at 1430 and 1670 cm^{-1} are attributed to δ_{as}(H–N–H) and δ_s(H–N–H) and the peaks at 3020 and 2810 cm^{-1} are attributed to ν_s(N–H) and ν_{as}(N–H), corresponding to the adsorption of NH_3 species on the Brønsted acid sites of the catalyst surfaces, respectively.[42] Characteristic peaks in different catalysts may shift slightly, which reflects changes in the N–H bonding energy after NH_3 adsorption.[33,42] For clarification, all corresponding peak wavenumber values of V*n*W/Ti are shown in Table 2.

The wavenumbers of all peaks corresponding to N–H bonds adsorbed on Brønsted acid sites decrease from V1W/Ti to V9W/Ti and increase from V9W/Ti to V13W/Ti, which indicates that the interaction strength of the N–H bonds of the NH_3 species absorbed on the Brønsted acid sites decreases first and then increases. However, the changing trend of the wavenumbers of the peaks corresponding to N–H bonds adsorbed on the Lewis acid sites does not show obvious regularity. Combined with the Raman and XPS results, the interaction strength of the V=O

Table 2 Wavenumbers of acid sites on the V*n*W/Ti catalysts at 50 °C[a]

Type	Brønsted acid site wavenumber (cm^{-1})				Lewis acid site wavenumber (cm^{-1})		
Vibration mode	ν_s(N–H)	ν_{as}(N–H)	δ_s(H–N–H)	δ_{as}(H–N–H)	ν_s(N–H)	δ_{as}(H–N–H)	δ_s(H–N–H)
V1W/Ti	3038	2849	1695	1462	3212	1596	1185
V3W/Ti	3030	2849	1695	1458	3199	1599	1176
V5W/Ti	3021	2833	1678	1455[a]	3251	1603	1230
V7W/Ti	3020	2825	1672	1451[b]	3250	1609	1230
V9W/Ti	3011	2800	1672	1448	3232	1599	1246
V11W/Ti	3030	2825	1680	1462	3219	1596	1246
V13W/Ti	3032	2826	1681	1462	3216	1596	1229

[a] a and b: pyrolysis peak.

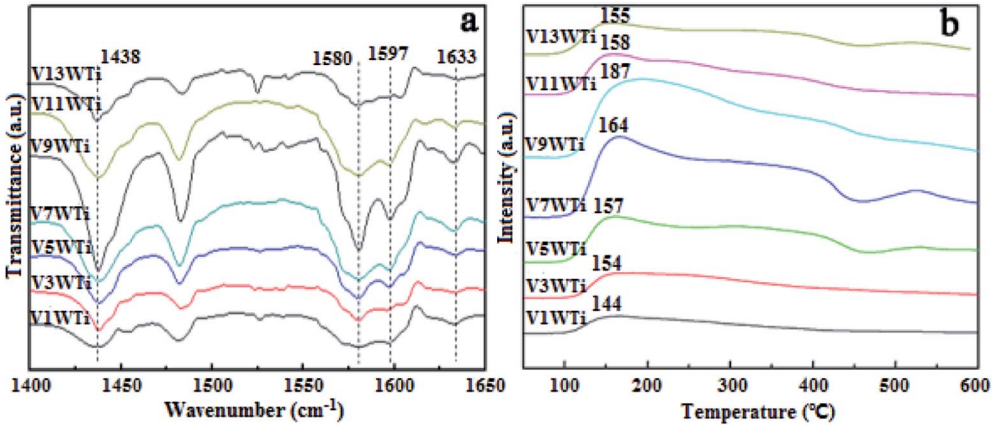

Fig. 5 Pyridine *in situ* IR spectra and NH_3-TPD profiles of the V*n*W/Ti catalysts at 50 °C.

bond increases with increasing V^{4+}/V^{5+} ratio, resulting in enhanced interactions between V=O and NH_3 (V^{5+}–$O^{-}\cdots H\cdots{}^{+}NH_3$) and a decrease of the N–H stretching vibration of adsorbed NH_3; therefore, the peak shifts to a lower wavenumber. When the vanadium loading exceeds 9%, crystalline V_2O_5 forms on the surface of the catalyst and the V^{4+}/V^{5+} ratio begins to decrease. The V=O stretching vibration is weak, resulting in a weakened link between V=O and NH_3; therefore, the N–H stretching vibration of adsorbed NH_3 increases slightly.

In order to further investigate the effects of changes in the V^{4+}/V^{5+} ratio on the Brønsted acid and Lewis acid sites of the catalyst surface caused by different vanadium loadings, pyridine adsorption IR and NH_3-TPD tests of the catalysts with different vanadium contents were performed. The infrared spectra of pyridine adsorbed on V*n*W/Ti with different vanadium contents at 50 °C are shown in Fig. 5(a), and the NH_3-TPD spectra are shown in Fig. 5(b). The peaks at 1580 and 1633 cm^{-1} belong to Brønsted acid sites, and the peaks at 1597 and 1438 cm^{-1} are attributed to Lewis acid sites.[45] The peak intensity increased first and then decreased with

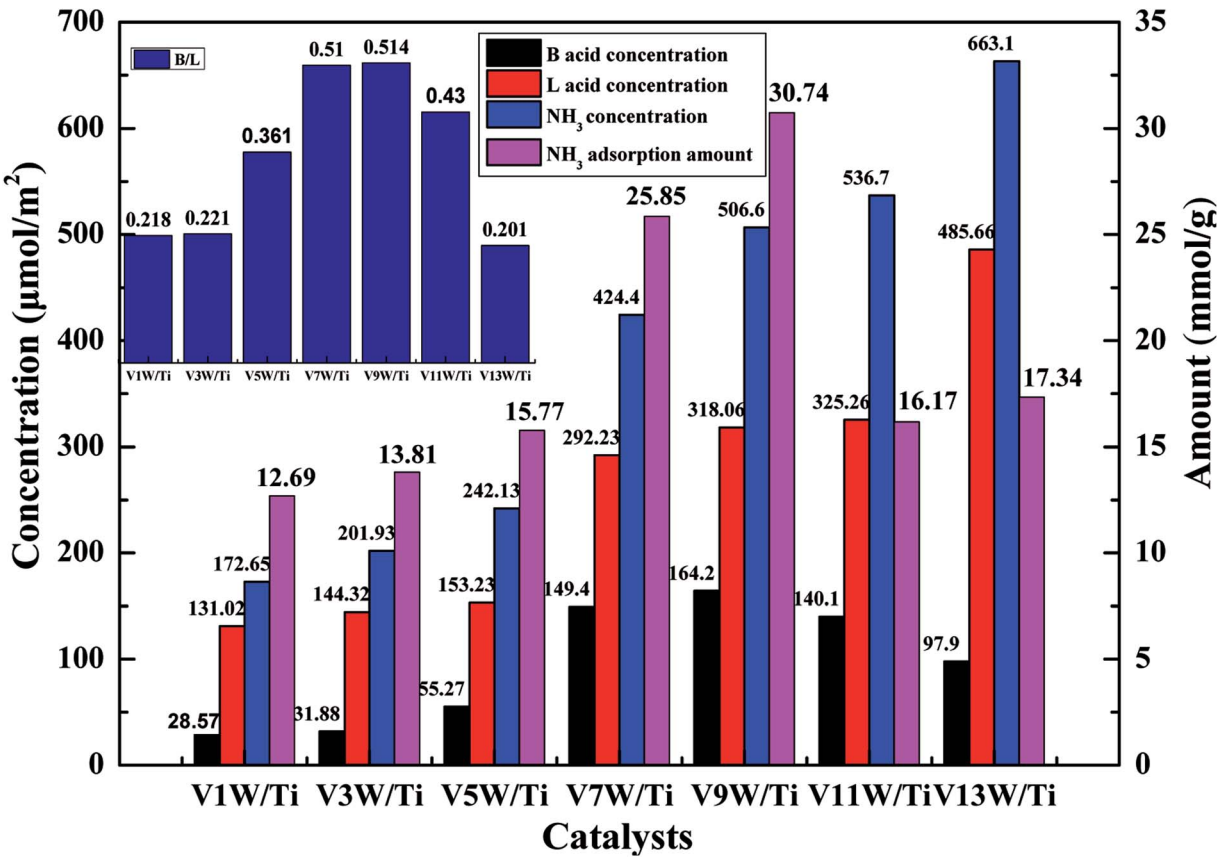

Fig. 6 Numbers of acid sites per unit area and total amounts of NH_3 for the V*n*W/Ti catalysts at 50 °C.

increasing vanadium content, and it reached the maximum value when the vanadium content was 9 wt%. The ratios of Brønsted acid and Lewis acid sites (B/L) calculated from the infrared characteristic peak areas, the numbers of acid sites per unit area and the total NH_3 adsorption amounts calculated from the NH_3-TPD peak areas are presented in Fig. 6. The results show that the numbers of B acid sites per unit area and the B/L values are in accordance with the NH_3 adsorption capacity and reach the maximum value when the vanadium loading reaches 9%. At this point, the V9W/Ti catalyst exhibits the best catalytic activity. Correspondingly, the vanadium species on the support surface are in transition from the aggregation state to the crystalline state, and V^{4+}/V^{5+} reaches the maximum value. The B/L and total amount of NH_3 adsorption begin to decrease obviously in the catalysts with vanadium loadings of 11% and 13%. It can be inferred that the V^{4+}/V^{5+} ratio is related to the number of B acid sites on the surface and that the formation of crystalline vanadium oxide has a negative effect on surface acidity. These results are consistent with previous tests. Interestingly, although the total amount of NH_3 adsorption decreases, the amount of NH_3 adsorbed and the L acid site per unit area continue to increase, which may be due to a large amount of crystallization of vanadium species on the support surface. In addition, this is related to a significant decrease in the specific surface area.

Attack of NO + O_2 on the adsorbed NH_3 was studied as follows, and the *in situ* IR spectra of the V*n*W/Ti catalysts are shown in Fig. 7 and Fig. 8. The test conditions were an atmosphere of 1000 ppm NO and 5 vol% O_2/Ar at various times after adsorption of 1000 ppm NH_3/Ar at 200 °C for 30 min. Some peaks appeared after adsorption of NH_3 at 3038, 2810, 1695, 1462 cm^{-1}; these are attributed to V^{5+}–$O^{-}\cdots{}^{+}H_3N\cdots$H–O–$V^{4+}$.[43,44] The existence time of the transition state reflects the speed of the SCR reaction. Under attack of NO + O_2, all the characteristic peaks disappeared gradually over time. NH_3 adsorbed on V9W/Ti with the highest V^{4+}/V^{5+} ratio exhibited the best catalytic performance, and no NH_3 characteristic peaks could be observed after 5 min of reaction. This is consistent with the results of the activity tests below. For the V11W/Ti, V7W/Ti, V5W/Ti, V3W/Ti and V1W/Ti catalysts, the NH_3 species were consumed completely after 9, 9, 10, 13 and 15 min, respectively. Therefore, the reactivity of adsorbed NH_3 on the catalysts is in the order of V9W/Ti > V11W/Ti > V7W/Ti > V5W/Ti > V3W/Ti > V1W/Ti. In fact, macroscopic changes in the vanadium loading lead to microscopic changes in the V^{4+}/V^{5+} ratio, regularly, and eventually indicate changes in the activation energy (E_a). Artificial regulation of vanadium loading to properly increase the V^{4+}/V^{5+} content may replace the process of electron transfer between vanadium species, accelerating the disappearance of the transition state; this enhances the NH_3-SCR

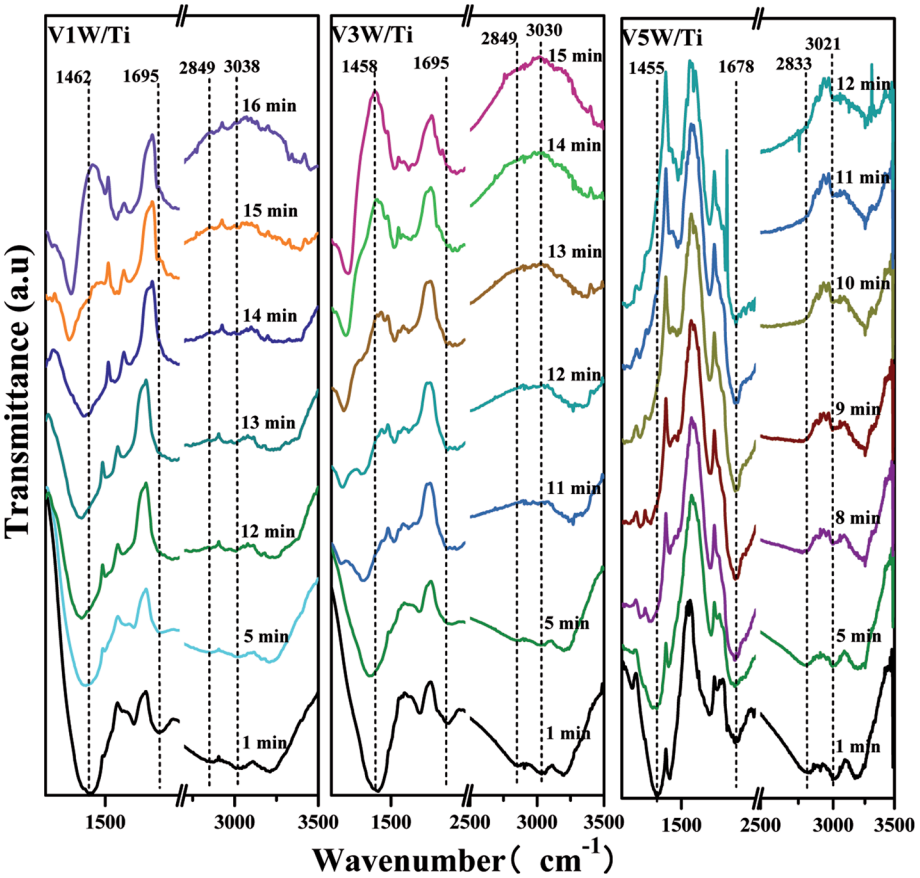

Fig. 7 *In situ* IR spectra of the V*n*W/Ti ($n = 1, 3, 5$) catalysts under an atmosphere of 1000 ppm of NO and 5 vol% O_2/Ar at different times after adsorption of 1000 ppm of NH_3/Ar at 200 °C for 30 min.

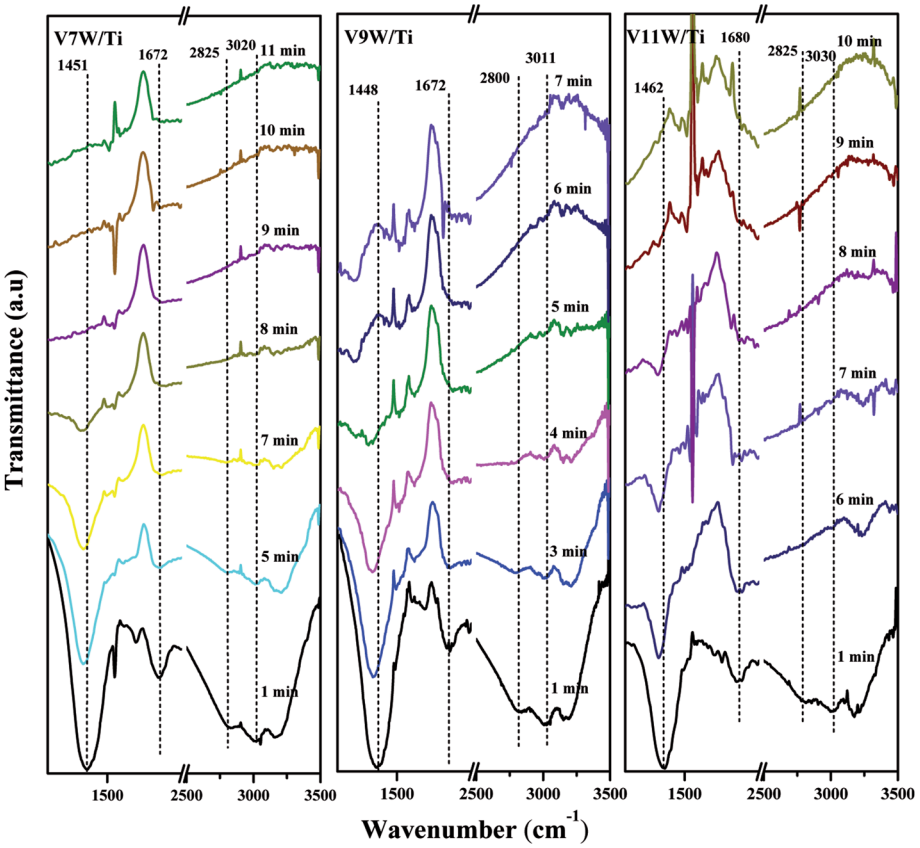

Fig. 8 *In situ* IR spectra of the V*n*W/Ti (n = 7, 9, 11) catalysts under an atmosphere of 1000 ppm of NO and 5 vol% O_2/Ar at different times after adsorption of 1000 ppm of NH_3/Ar at 200 °C for 30 min.

reaction performance. The E_a for forming the transition state decreased as the vanadia loading amount increased and reached a minimum value for the V9W/Ti catalyst, which has the highest V^{4+}/V^{5+} ratio; this indicates that the Brønsted acid sites on transition state vanadium enhance the reactivity of NH_3. When crystalline V_2O_5 is formed on the catalyst surface, a large amount of V^{5+} appears and the V=O and V–O bonding energies decrease, resulting in weak interactions between the Brønsted acid sites (V^{5+}–O–H) and NH_3; therefore, the N–H stretching vibration of the adsorbed NH_3 strengthens and, finally, E_a increases. It can be inferred that changes in the proportion of active components on the support surface profoundly affect the multiphase reaction process.

3.4 Redox properties of the catalysts

It has been reported[29] that the oxidative dehydrogenation of ammonia species adsorbed by vanadia species is a key step in the SCR reaction. To investigate the redox capacity of vanadium ions with changing V^{4+}/V^{5+} ratio, temperature programmed reduction (H_2-TPR) and temperature programmed oxide (O_2-TPO) spectra were obtained and are shown in Fig. 9.

The peaks at 536 °C to 610 °C are ascribed to the reduction of vanadia, corresponding to the reduction of V^{5+} to V^{3+} and of V^{4+} to V^{3+}.[38,46] The stability of V_2O_3 did not decrease even at a higher temperature.[47] The reduction temperature moves in the direction of low temperature from V1W/Ti to V5W/Ti and moves in the direction of high temperature in the range of V7W/Ti to V13W/Ti. The high dispersion of vanadium species with a small amount of V^{4+} on the support surface enhances the interaction between the vanadium species and the support. Therefore, the reduction temperature is higher. When the vanadium content is less than 5%, with increasing vanadium loading, the interaction between the vanadium species gradually strengthens and the interaction between vanadium and support weakens. This leads to a gradual decrease in the reduction temperature. When the vanadium loading is higher than 5%, the V^{4+}/V^{5+} ratio increases significantly and polymeric and crystalline vanadia species, which are difficult to reduce, form on the support surface,[48,49] resulting in an increase in the reduction temperature; this is consistent with the Raman results. In addition, two reduction peaks appear in the catalysts with 11 wt% and 13 wt% vanadium loading amounts; these correspond to the reduction of dispersed, polymeric and crystalline vanadia species[50] coexisting on the catalyst surface,[51] respectively. It must be noted that this change in the dispersion status is consistent with the trend of V^{4+}/V^{5+}. Moreover, tungsten oxide is difficult to reduce; the reduction peak of WO_3 appears at around 654 °C in W/TiO_2, but it does not appear at the same temperature position in the V*n*W/Ti catalyst. We believe that the reduction peak of WO_3 in the V*n*W/Ti catalyst moves toward a higher temperature. This may be due to the interaction between vanadium and tungsten species.

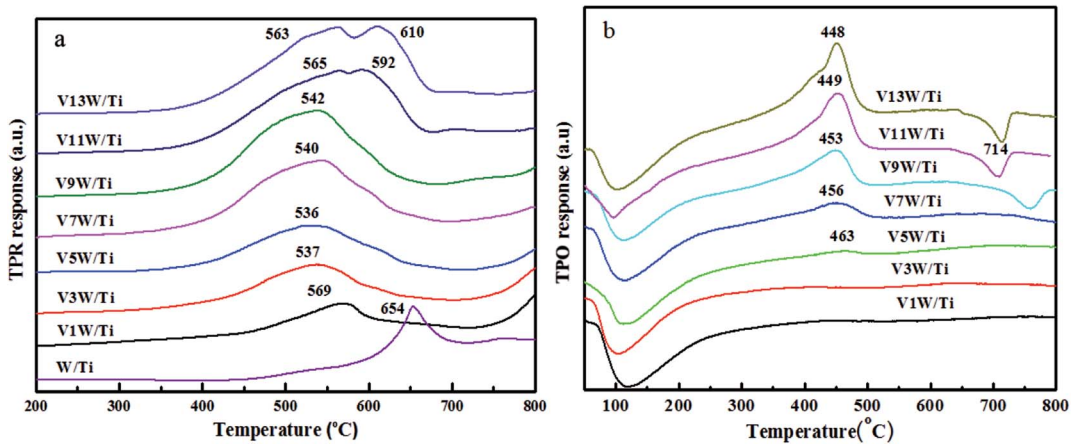

Fig. 9 H_2-TPR profiles (a) and O_2-TPO profiles (b) of the V*n*W/Ti catalysts.

The TPO results further illustrate that the vanadia species on the catalyst surface have been reduced to V_2O_3,[46] as shown in Fig. 9(b). Therefore, the peaks at 448 °C to 463 °C belong to the oxidation of V_2O_3, corresponding to the oxidation of V^{3+} to V^{4+} and then to V^{5+}.[49] The peak at around 100 °C may be caused by residual water. When the loading amount of vanadium oxide increases from 1 wt% to 5 wt%, strong interactions between the highly dispersed vanadium oxide and the support result in a broader oxidation peak, and no maximum oxidation peak appears. A large number of aggregated vanadium oxides form when the vanadium oxide loading amount exceeds 5 wt%; therefore, the amount of V_2O_3 on the catalyst surface increases after H_2-TPR under these conditions. The oxidation peak temperature decreases due to the weakened interactions between vanadium and the support. The decreased peak at 714 °C is attributed to the restraint of melting V_2O_5 to oxygen diffusion on the catalyst surface when the vanadium oxide loading amount exceeds 9 wt%. In order to more clearly analyze the redox properties of a series of catalysts, quantitative analysis of the TPR and TPO results has been further conducted as follows.

The H_2 and O_2 consumption and the oxidation and reduction rates (ν_{TPO} and ν_{TPR}, respectively) of the catalysts are listed in Table 3. The increased H_2 and O_2 consumption is due to the continuous addition of vanadium species to the support surface. For the reduction process, the dispersed vanadium species on the catalyst surface are difficult to reduce at low vanadium loadings due to the strong interactions between vanadium and the support. This interaction weakens as the vanadium loading increases, and the reduction rate improves during this process. The oxidation process is similar to the reduction process. The increase of the reduction rate is faster than that of the oxidation rate at low loading amounts; however, the two are exactly opposite at high loading amounts due to the appearance of polymeric or crystalline vanadia when the loading amount of vanadium oxide exceeds 9 wt%. This result is coincident with the previous conclusion[49] that crystalline and polymeric vanadia are difficult to reduce but readily oxidized after reduction, while dispersive vanadia is readily reduced but difficult to oxidize after reduction.

Table 3 H_2 consumption, O_2 consumption and redox properties of the V*n*W/Ti catalysts

	Consumption (μmol g^{-1})		N(mol m^{-2} s^{-1}) $\times 10^{-9}$		
Sample	H_2	O_2	ν_{TPR}	ν_{TPO}	E_a (kJ mol^{-1})
V1W/Ti	289	165	2.37	0.95	25.1
V3W/Ti	523	200	3.70	1.23	21.7
V5W/Ti	710	220	4.62	1.42	21.4
V7W/Ti	958	308	7.55	2.13	20.5
V9W/Ti	1120	416	8.65	2.92	15.7
V11W/Ti	1150	605	8.82	7.68	16.1
V13W/Ti	1180	652	1.10	1.01	16.6

3.5 DeNO$_x$ activity and macrokinetics

Fig. 10 shows the deNO$_x$ activities of the V*n*W/Ti catalysts and Fig. 11 shows the Arrhenius plots of the intrinsic reaction rate constants, the V^{4+}/V^{5+} ratios and the E_a values of the V*n*W/Ti catalysts. With increasing vanadium loading, the content of vanadium species with different valencies increases; however,

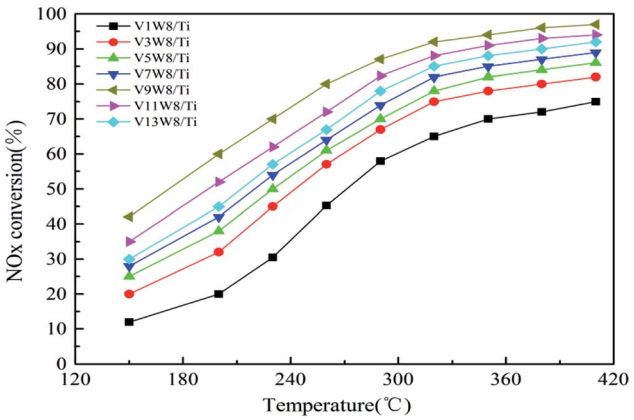

Fig. 10 The deNO$_x$ activities of the V*n*W/TiO$_2$ catalysts.

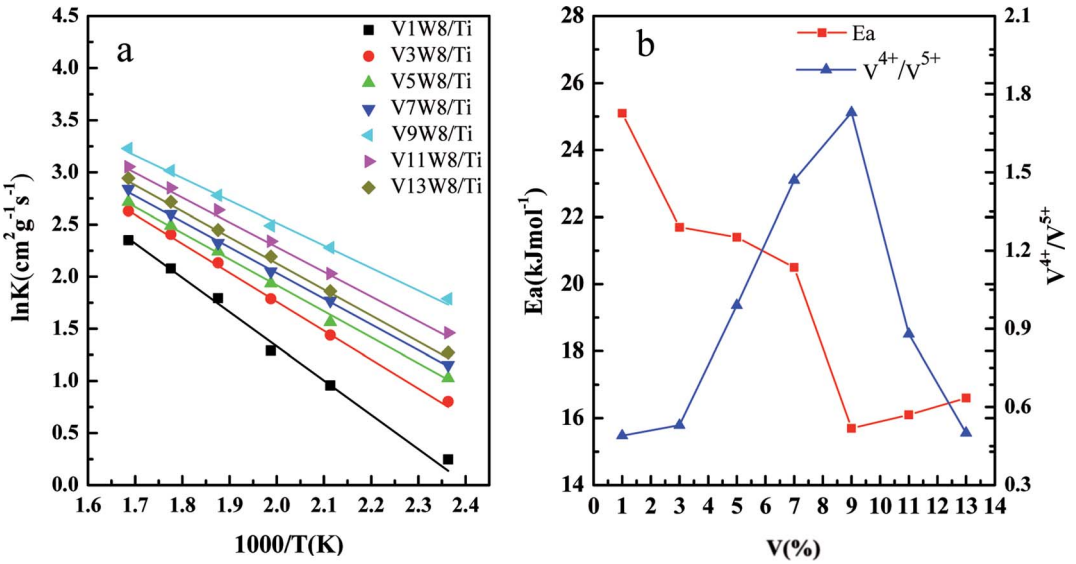

Fig. 11 Arrhenius plots of the intrinsic reaction rate constants of the V*n*W/TiO$_2$ catalysts (a) and the relationship between the V^{4+}/V^{5+} ratios of the catalysts and the apparent activation energies (E_a) (b).

the SCR performance does not always improve. The catalytic activity shows a regular change, increasing first and then decreasing, which is related to the V^{4+}/V^{5+} ratio. When the loading reaches 9%, the deNO$_x$ activity is the best; meanwhile, the V^{4+}/V^{5+} ratio reaches the maximum value.

The deNO$_x$ reaction macrokinetics for the V*n*W/Ti catalyst were determined to realize the intrinsic effects of the V^{4+}/V^{5+} ratio on the catalyst activity. In order to avoid diffusion effects on the catalytic activity, steady-state conditions experiments were carried out at a high space velocity of 300 000 h^{-1} in the temperature range of 150 °C to 320 °C.

The NH_3-SCR reaction on a V*n*W/Ti catalyst is normally regarded as a first order reaction with respect to NO.[52–54] The rate equation is $r = kc_{NO}$ and the rate constant can be described by eqn (3)–(5):

$$-r_{NO} = k_{NO}c_{NO,0}(1 - x_{NO}) = \frac{F_{NO,0}\mathrm{d}x_{NO}}{\mathrm{d}V_{cat}} \quad (3)$$

$$-V_a \ln(1 - x_{NO}) = k_{NO} \quad (4)$$

$$k = A \exp\left(-\frac{E_a}{RT}\right) \quad (5)$$

where k_{NO} is the reaction rate coefficient (s^{-1}), $F_{NO,0}$ is the NO feed rate (mL s^{-1}), $c_{NO,0}$ is the NO molar concentration (mol mL^{-1}) at the inlet, V_a is the space velocity (s^{-1}), V_{cat} is the accumulation volume of the catalyst (mL), the stacking densities of the catalysts are 0.641, 0.645, 0.650, 0.662, 0.735, 0.821, and 0.912 g mL^{-1}, corresponding to 1 wt% to 13 wt% vanadia content, respectively, x_{NO} is the NO conversion (%), A is the pre-exponential factor, E_a is the apparent activation energy (kJ mol^{-1}), R is the gas constant (8.3145 J mol^{-1} K^{-1}) and T is the temperature (K).

Fig. 11(a) shows the Arrhenius plots based on the reaction rate data, and the E_a values were determined from the plots (Table 2). Fig. 11(b) shows the relationship between the V^{4+}/V^{5+} ratios of the V*n*W/Ti catalysts and their E_a values. As shown in Fig. 11(b), the value of E_a has a tendency to increase initially and then decrease with increasing vanadia loading. Also, it reaches the minimum when the content of vanadia is 9 wt%. Accordingly, in Fig. 11(b), the value of E_a has the same tendency with the variation of the V^{4+}/V^{5+} ratio, where E_a increases initially and then decreases with changing V^{4+}/V^{5+} ratio and reaches the minimum when the V^{4+}/V^{5+} ratio is the maximum. Furthermore, the catalyst with 9 wt% vanadia loading amount shows the highest deNO$_x$ activity, which indicates that increasing the V^{4+}/V^{5+} ratio can decrease the E_a and enhance the deNO activity.

4 Conclusion

In this study, the contents of vanadium with different valencies on a support surface have been controlled by adjusting the vanadium loading; also, the relationship between the V^{4+}/V^{5+} ratio and vanadium dispersion on the support surface, the concentration of chemically adsorbed oxygen, the surface acidity and the catalytic activity has been established. Although the contents of V^{4+} and V^{5+} gradually increase during the addition of vanadium, the catalytic activity shows a highly regular change. Changing the ratio of V^{4+}/V^{5+} is a key factor in controlling the catalytic activity than the absolute contents of V^{4+} and V^{5+}. When the loading reaches 9%, the deNO$_x$ activity is the best; meanwhile, the V^{4+}/V^{5+} ratio reaches the maximum value and the appearance energy (E_a) required for forming the SCR reaction transition state is the lowest. In addition, the change trend of V^{4+}/V^{5+} is very close to the variation trend of the dispersion state of the vanadium species, the concentration of chemically adsorbed oxygen and the surface acidity. Different ratios of V^{4+}/V^{5+} represent different dispersion states of vanadium species, and changes in this ratio affect the interactions between V, W, O and Ti atoms; this is the main

reason why the best catalytic activity is observed when the V^{4+}/V^{5+} ratio reaches its maximum value.

Conflicts of interest

The authors declare no conflicts of interest.

Abbreviations

NH_3-SCR	Selective catalytic reduction
XRD	X-ray diffraction
XPS	X-ray photoelectron spectroscopy
H_2-TPR	H_2 temperature programmed reduction
O_2-TPO	O_2 temperature programmed oxidation
E_a	Apparent activation energy

Acknowledgements

This work was supported by the Fundamental Research Funds for the Central Universities (No. HEUCF20151016), Heilongjiang Province Science Foundation Project Plan (Grant No. E2017027), the Fundamental Research Funds for the Central Universities of Harbin Engineering University (Grant No. HEUCFP201802) and Advanced Technique Project Funds of the Manufacture and Information Ministry.

Notes and references

1 G. Busca, M. A. Larrubia and L. A. G. Ramis, *Catal. Today*, 2005, **107**, 139–148.
2 G. Busca, L. Lietti, G. Ramis and F. Berti, *Appl. Catal., B*, 1998, **18**, 1–36.
3 P. Forzatti, I. Nova, E. Tronconi, A. Kustov and J. R. Thøgersen, *Catal. Today*, 2012, **184**, 153–159.
4 L. Gan, J. Chen, Y. Peng, J. Yu, T. Tran, K. Li, D. Wang, G. Xu and J. Li, *Ind. Eng. Chem. Res.*, 2018, **57**, 150–157.
5 Z. Liu, S. Zhang, J. Li, J. Zhu and L. Ma, *Appl. Catal., B*, 2014, **158–159**, 11–19.
6 Z. Ma, X. Wu, Y. Feng, Z. Si, D. Weng and L. Shi, *Prog. Nat. Sci.: Mater. Int.*, 2015, **25**, 342–352.
7 S. Djerad, L. Tifouti, M. Crocoll and W. Weisweiler, *J. Mol. Catal. A: Chem.*, 2004, **208**, 257–265.
8 S. B. Kristensen, A. J. Kunov-Kruse, A. Riisager, S. B. Rasmussen and R. Fehrmann, *J. Catal.*, 2011, **284**, 60–67.
9 G. W. Coluston, S. R. Bare, H. Kung, K. Birkeland, G. K. Bethke, R. Harlow, N. Herron and P. L. Lee, *Science*, 1997, **275**, 191–193.
10 G. Centi, F. Trifiro, J. R. Ebner and V. M. Franchetti, *Chem. Rev.*, 1988, **88**, 55–80.
11 M. P. House, A. F. Carley and M. Bowker, *J. Catal.*, 2007, **252**, 88–96.
12 Y. Cai and U. Ozkan, *Appl. Catal.*, 1991, **78**, 241–255.
13 J. Due-Hansena and S. B. Rasmussen, *Appl. Catal., B*, 2011, **107**, 340–346.
14 G. C. Bond and S. F. Tahir, *Appl. Catal.*, 1991, **71**, 1–31.
15 G. Deo and I. E. Wachs, *J. Catal.*, 1994, **146**, 323–334.
16 I. E. Wachs, G. Deo, B. M. Weckhuysen, A. Andreini, M. A. Vuurman, M. De Boerand and M. D. Amiridis, *J. Catal.*, 1996, **161**, 211–221.
17 S. T. Choo, Y. G. Lee, I. S. Nam, S. W. Ham and J. B. Lee, *Appl. Catal., A*, 2000, **200**, 177–188.
18 G. T. Went, L. J. Leu and A. T. Bell, *J. Catal.*, 1992, **134**, 479–491.
19 G. T. Went, L. J. Leu and A. T. Bell, *J. Catal.*, 1992, **134**, 492–505.
20 G. J. Dong, Y. Zhao and Y. F. Zhang, *J. Fuel Chem. Technol.*, 2014, **42**, 1093–1101.
21 G. J. Dong, Y. Bai, Y. F. Zhang and Y. Zhao, *New J. Chem.*, 2015, **39**, 3588–3596.
22 M. J. Lázaro, A. Boyano, C. Herrera, M. A. Larrubia, L. J. Alemany and R. Moliner, *Chem. Eng. J.*, 2009, **155**, 68–75.
23 I. E. Wachs and C. A. Roberts, *Chem. Soc. Rev.*, 2010, **39**, 5002–5017.
24 M. A. Vuurman, I. E. Wachs and A. M. Hirt, *J. Phys. Chem.*, 1991, **95**, 9928–9937.
25 A. Khodakov, B. Olthof, A. T. Bell and E. Iglesia, *J. Catal.*, 1999, **181**, 205–216.
26 G. T. Went, S. T. Oyama and A. T. Bell, *J. Phys. Chem.*, 1990, **94**, 4240–4246.
27 I. Giakoumelou, C. Fountzoula, C. Kordulis and S. Boghosian, *J. Catal.*, 2006, **239**, 1–12.
28 G. C. Bond, *Appl. Catal., A*, 1997, **157**, 91–103.
29 F. Tang, K. Zhuang, F. Yang, L. Yang, B. Xu, J. Qiu and Y. Fan, *Chin. J. Catal.*, 2012, **33**, 933–940.
30 G. Dong, Y. Zhang, Y. Zhao and Y. Bai, *New J. Chem.*, 2015, **39**(5), 3588–3596.
31 E. I. Wachs and M. B. Weckhuysen, *Appl. Catal., A*, 1997, **157**, 67–90.
32 K. Cheng, J. Liu, T. Zhang, J. M. Li, Z. Zhao, Y. C. Wei, G. Y. Jiang and A. J. Duan, *J. Environ. Sci.*, 2014, **26**, 2106–2133.
33 G. J. Fang, K. L. Yao and Z. L. Liu, *Thin Solid Films*, 2001, **394**, 63–70.
34 M. Najbar, E. Broclawik, A. Gora, J. Camrac, A. Białas and A. Wesełucha-Birczyńska, *Chem. Phys. Lett.*, 2000, **325**, 330–339.
35 E. Broclawik, A. Gora and M. Najbar, *J. Mol. Catal. A: Chem.*, 2001, **166**, 31–38.
36 M. A. Eberhardt, A. Proctor, M. Houalla and D. M. Hercules, *J. Catal.*, 1996, **160**, 27–34.
37 M. Demeter, M. Neumann and W. Reichelt, *Surf. Sci.*, 2000, **454**, 41–44.
38 P. G. W. A. Kompio, A. Brückner, F. Hipler, G. Auer, E. Löffler and W. Grünert, *J. Catal.*, 2012, **286**, 237–247.
39 S. L. Zhang and Q. Zhong, *J. Mol. Catal. A: Chem.*, 2013, **373**, 108–113.
40 M. Najbar, E. Broclawik, A. Góra, J. Camra, A. Bialas and A. Weselucha-Bircayńska, *Chem. Phys. Lett.*, 2000, **325**, 330.
41 C. Liang and J. Li, *Chem. Eng. J.*, 2011, **170**, 531–537.
42 M. A. Centeno, I. Carrizosa and J. A. Odriozola, *Appl. Catal., B*, 2001, **29**, 307–314.

43 N.-Y. Topsoe, *Science*, 1994, **265**, 1217–1219.
44 N.-Y. Topsoe and J. A. Dumesic, *J. Catal.*, 1995, **151**, 241–252.
45 S. Yamazoe, Y. Masutani, K. Teramura, Y. Hitormi, T. Shishido and T. Tanaka, *Appl. Catal., B*, 2008, **83**, 123–130.
46 W. C. Yu, X. D. Wu, Z. C. Si and D. Weng, *Appl. Surf. Sci.*, 2013, **283**, 209–214.
47 F. Klose, T. Wolff, H. Lorenz, A. Seidel-Morgenstern, Y. Suchorski, M. Piórkowska and H. Weiss, *J. Catal.*, 2007, **247**, 176–193.
48 C. Z. Wang, S. J. Yang, H. Z. Chang, Y. Peng and J. H. Li, *Chem. Eng. J.*, 2013, **225**, 520–527.
49 S. Besselmann, C. Freitag, O. Hinrichsen and M. Muhler, *Phys. Chem. Chem. Phys.*, 2001, **3**, 4633–4638.
50 A. Khodakov, B. Olthof, A. T. Bell and E. Iglesia, *J. Catal.*, 1999, **181**, 205–216.
51 X. D. Wu, W. C. Yu, Z. C. Si and D. Weng, *Front. Environ. Sci. Eng.*, 2013, **7**, 420–427.
52 X. Guo, C. Bartholomew, W. Hecker and L. L. Baxter, *Appl. Catal., B*, 2009, **92**, 30–40.
53 J. P. Chen and R. T. Yang, *Appl. Catal., A*, 1992, **80**, 135–148.
54 K. Kamasamudram, N. W. Currier, X. Chen and A. Yezerets, *Catal. Today*, 2010, **151**, 212–222.